

Article

Structure Simulation and Host–Guest Interaction of Histidine-Intercalated Hydrotalcite–Montmorillonite Complex

Chen-Xi Wang, Min Pu * , Pei-Huan Zhang, Yang Gao, Zuo-Yin Yang and Ming Lei

State Key Laboratory of Chemical Resource Engineering, Beijing University of Chemical Technology, Beijing 100029, China; lcuwangchenxi@163.com (C.-X.W.); zhangph1107@126.com (P.-H.Z.); yh1201gaoyang@163.com (Y.G.); yangzy@mail.buct.edu.cn (Z.-Y.Y.); leim@mail.buct.edu.cn (M.L.)

* Correspondence: pumin@mail.buct.edu.cn; Tel.: +86-010-64425385

Received: 20 March 2018; Accepted: 25 April 2018; Published: 07 May 2018



Abstract: The structures of histidine intercalated hydrotalcite–montmorillonite complex (His–LDHs–MMT) were studied using the DMol3 code, GGA/PW91 function, and DND basis set of the density functional theory (DFT). The geometries of His–LDHs–MMT were optimized, and their electronic properties were calculated. The results showed that the structure of the complex can be seen as that the quaternary ammonium group of histidine was adsorbed on the oxygen of MMT lamella, and its oxygen on the carboxylic acid anion was combined with the hydrogen atoms of the LDHs lamella. It was determined that the interaction mainly consisted in hydrogen bonding and electrostatic force. The average binding energies per histidine of His–LDHs and His–MMT were about -65.89 and -78.44 kcal/mol, respectively. The density of states of the complexes showed that the 2p orbitals of oxygen were dominant, and the 1s orbit of hydrogen near the Fermi level indicate the formation of hydrogen bonds in the complex. The charge density data displayed the density field of histidine carboxylic acid anion overlapped with that of hydrotalcite layer, indicating that a strong hydrogen bond interaction existed between histidine and hydrotalcite layer. The analysis of the electrostatic potential of complex indicated that the electrostatic interaction between histidine and MMT is obviously stronger than that of LDHs. The simulated XRD spectra showed the special diffraction peaks of LDHs and MMT layer in the complex.

Keywords: hydrotalcite; montmorillonite; histidine; structure simulation; DFT; interaction

1. Introduction

Hydrotalcite and montmorillonite are anionic and cationic clay minerals that occur in nature, respectively. Hydrotalcites (LDHs) [1] are mainly composed of metal dihydroxide lamellae and interlayer anions, and are widely used in the fields of catalysis [2–4], pharmaceuticals [5,6], functional materials [7–9], and environmental protection [10,11]. Montmorillonite (MMT) is one of a kind of layered aluminosilicate and has the good properties of thermal insulation and gas-liquid dielectric barrier. It is widely used in the pollution control [12–15], petrochemical industry [16–18], and others [19]. The structure of the LDHs lamella is similar to that of brucite, in which the Mg^{2+} of layer is partially replaced by Al^{3+} [20–22], so that the excess positive charge of the layer requires the anion to balance. On the other hand, the MMT lamellae that may be considered as Al^{3+} is partially replaced by Mg^{2+} ions in the aluminosilicate. The cations are needed to balance the electrical charges of MMT lamellae. Both the LDHs and MMT lamellae of complexes need the opposite charged ion to retain the electrical neutrality in one supermolecule. The amphoteric ion characteristics indicate that amino acid zwitterion will be the best guest for linking the LDHs and the MMT host [23].

Because the electrostatic attraction occurs between opposite electrical charges, according to the charged nature of LDHs and MMT lamellae, the intercalated complex materials may be obtained using the self-assembled intercalation method of zwitterions. This is one kind of new intercalated material with an acid–base bifunctional structure. LDHs and MMT are layered materials that exist in nature and are cheap and readily available, which is conducive to the full use of natural resources for sustainable development of the environment. It is believed that this field will make great progress in the near future. Histidine contained an imidazole ring that has been widely used as the catalyst for the Aldol reaction [24,25] and the Baylis–Hillman reaction [26,27]. In addition, it is also used in the fields of physiology, medicine [28–31], and chemical industry [32–34]. When the histidine is intercalated into the layers of LDHs and MMT, it acts as a pillar support and the stability of the lamellae increases. In addition, the unique properties of histidine can enhance the reactivity of the complex material as a carrier or catalyst. Since the imidazole ring of histidine has high proton conductivity, it may be used as an electrolyte in electrochemical materials [35,36]. Recent years, there has been much research about amino acids intercalated-LDHs and MMT [37–43]. However, the studies about histidine-intercalated LDHs–MMT complexes have not been seen in the literature to the best of our knowledge. In this article, histidine as an amphiphilic ion is selected as the intercalated guest.

Aisawa et al. [37] used the co-precipitation method to synthesize some phenylalanine, glycine, and oligopeptides-intercalated Zn–Al LDHs. The effects of different pH on the co-precipitation were investigated, and the pH = 8–9 was the most suitable for preparing oligopeptide and amino acids-intercalated LDHs. Infrared, Raman and XRD spectroscopy showed that amino acids intercalated well between LDHs. Nakayama et al. [38] described some amino acids (leucine and phenylalanine), and oligopeptides were intercalated into Mg–Al LDHs in the alkaline solution by the calcination-rehydration method. The most appropriate intercalated amount of amino acid was measured at about 2 mmol amino acids per 0.56 g LDHs. Whilton et al. [39] synthesized glutamic acid, aspartic acid, and polyaspartic acid-intercalated Mg–Al LDHs using the co-precipitation method, and the obtained interlayer spacing was about 1.5 nm. Fudala et al. [40] prepared the phenylalanine and tyrosine intercalated Zn–Al LDHs and MMT using the ion exchange method, respectively. According to XRD and infrared spectroscopy, it can be found that the interlayer spacing of the material increased after the intercalation of amino acid, and an interaction existed between the hydrotalcite host and guest. Yuan et al. [41] studied the preparation and pyrolysis of aspartate/Mg–Al LDHs and phenylalanine/M²⁺–Al LDHs. The structure and composition of the intercalation material were characterized by X-ray diffraction, inductively coupled plasma atomic emission spectrometry, and elemental analysis. They determined that the amino acids were successfully intercalated into LDHs layers, and the carboxylate anion of the amino acid forms a hydrogen bond with the LDHs lamella.

Norio et al. [42] studied the adsorption properties and the effects of different pH values of L-lysine in MMT using ATR-IR. They showed that when pH = 4.9–9.7, the MMT surface can adsorb lysine electrostatically. Mallakpour et al. [43] investigated the effects of L-Ala, L-Val, L-Leu, L-Ile, L-Phe, and L-Met on the structure of Na MMT in aqueous solution and characterized the structure of products by means of XRD, TGA, FT-IR, SEM, FESEM and TEM. They determined that many amino acid molecules may be intercalated into the MMT layer well.

Fraser et al. [44] studied chiral differences in the effects of D- and L-histidine on the interlayer spacing of vermiculite clays. The results demonstrated that the effect of different enantiomers of an amino acid may alter physical and structural properties of clay systems at low amino acid concentrations and over a long length-range. Songurtekin et al. [45] reported the characterization and application of histidine-modified montmorillonite (His-MMT) in electrochemical biosensor fabrication. MMT modifications were followed by X-ray diffraction, Fourier transform infrared spectroscopy, zeta potential, and thermal gravimetry analysis. The experimental results showed that histidine was used as a modifier to enhance the immobilization capability of Mt for the biomolecules and applied successfully in both batch and FIA modes. The above references mainly described the preparation of

different amino acid-intercalated hydrotalcite or montmorillonite materials, so that they supported the basis for the theoretical study of the intercalated complex.

Our group had studied the structure of p-aminobenzene sulfonic acid-intercalated hydrotalcite–montmorillonite complex [46] and tried to explain the interactions between interlayer guest and the host lamella. The aim of this paper focuses on the interactions of interlayer guest and the host of histidine-intercalated hydrotalcite–montmorillonite complex (His–LDHs–MMT) theoretically. The structures and intercalation modes of His–LDHs–MMT complexes are calculated using the quantum chemical method. The XRD spectrum, interlayer forces, and electron properties of His–LDHs–MMT were analyzed.

2. Calculation Methods

All the structures of His–LDHs–MMT complexes are calculated using DMol3 code [47,48] of Material Studios 8.0. The geometries are optimized with GGA/PW91 function and DND basis set of the density functional theory (DFT) and using OBS method for DFT–D correction. The total DFT–D energy is a combination of atomic energies, kinetic, electrostatic, exchange correlation, spin polarization, and DFT–D correction. The SCF tolerance in the optimization is set as 1.0×10^{-5} , the max force as 0.04 Ha/nm, and max displacement as 0.0005 nm. The unit cell of complex is constructed with the LDHs–MMT layer (the ratio is 1:1) and histidine zwitterions. XRD of complex structure is simulated according to the principle of electron diffraction. Density of states and charge density of the complex are calculated with the optimized geometries.

The interaction between interlayer guests is calculated according to the Equations (1) and (2) as follows:

$$\Delta E(\text{His} - \text{His}) = E(\text{His1} - \text{His2}) - (E(\text{His1}) + E(\text{His2})), \quad (1)$$

$$\Delta E'(\text{His} - \text{His}) = \Delta E(\text{His1} - \text{His2})/2 \quad (2)$$

in which $\Delta E(\text{His} - \text{His})$ is the interaction energy between the interlayer guest, and $E(\text{His1})$ and $E(\text{His2})$ are the energy of histidines in a unit cell. $\Delta E'(\text{His} - \text{His})$ is the average of each histidine interaction energy.

The calculation formulas of binding energy of histidine-intercalated hydrotalcite or montmorillonite and the average binding energy $\Delta E'$ of each histidine of LDHs or MMT are shown in the following

$$\Delta E(\text{His} - \text{Layer}) = E(\text{His} - \text{Layer}) - (E(\text{His}) + E(\text{Layer})) \quad (3)$$

$$\Delta E'(\text{His} - \text{Layer}) = \Delta E(\text{His} - \text{Layer})/n(\text{His}) \quad (4)$$

In Equation (3), $\Delta E(\text{His} - \text{Layer})$ is the binding energy of histidine-intercalated LDHs, MMT, or complex layer; $E(\text{His} - \text{Layer})$ is the total energy of histidine intercalated LDHs, MMT, or LDHs–MMT; and $E(\text{His})$, $E(\text{Layer})$ are the energy of the histidine and LDHs, MMT, or LDHs–MMT lamellae, respectively. In Equation (4), $\Delta E'(\text{His} - \text{Layer})$ is the average binding energy of each histidine, and $n(\text{His})$ is the number of histidines in the unit cell.

3. Results and Discussion

3.1. Structural Analysis of His–LDHs–MMT Complex

Three possible structures (M1, M2, and M3) of His–LDHs–MMT complex are found in the potential energy surface. In the M1, M2, and M3 models, NH_3^- , COO^- group, and heterocyclic-N atoms of histidine combine with the H of LDHs and O atom of MMT, respectively. The optimized geometries of His–LDHs–MMT are shown in Figure 1. The unit cell parameters and total DFT–D energy of His–LDHs–MMT are listed in Table 1. In the LDHs lamellae, the Zn–O bond length is about 2.11 Å, and the Al–O bond length about 1.89 Å. In the MMT layer, the Si–O bond length is about 1.60–1.65 Å, the Al–O bond length about 1.97 Å, and the Mg–O bond length about 2.07 Å. These data are close to

the un-intercalated layer data. It shows that the layers of LDHs and MMT present a relative isolated and stable structure. The H–O or H–N interdistance of histidine intercalated LDHs are about 1.7–2.0 Å. The O–H distance of histidine intercalated MMT is about 1.7–2.5 Å. It hints that there are strong interactions between the host (LDHs and MMT) and guest (His). The H–O interdistance of the different His zwitterions in the M1, M2 is about 1.7–2.1 Å. It also means that an interaction exists between the interlayer guest, that is, His–His. It can be seen that both the interatomic distances of H with O and N in the unit cell of M1 and M2 are in the hydrogen bond length range, respectively. The simulations of the complex structures show that the oxygen on the carboxylate group is combined with the hydrogen atoms of the LDHs lamella, and the quaternary ammonium ion group of histidine is adsorbed with the oxygen of the MMT lamella. The flattening or upright arrangement modes of histidine between the layers can be founded out by comparing these three geometries. Histidines in the layers of M1 and M2 are almost flattening. Between M1 and M2, there exists the interaction between the histidine heterocyclic nitrogen atom and the LDHs in the M1, except for the hydrogen bond of the carboxylate oxygen of the amino acid with the LDHs lamella, which makes the binding of His and M1 lamellae more firm and stable than that of M2. The histidine of M3 is nearly upright between the lamellae, and there is little interaction between the guests of M3 layers. According to the unit cell data, the layer spacing and energy of M3 are higher than that of M1 and M2, which are regarded as not stable relative to the other two structures. It can be seen from the previous analysis that the histidine is linked by hydrogen bond between the layers of LDHs–MMT. M1 and M2 are the relatively stable structure of His–LDHs–MMT. M1 has more hydrogen bonding of heterocyclic nitrogen with the LDHs lamellae than M2, which makes the adsorption strong and the structure stable.

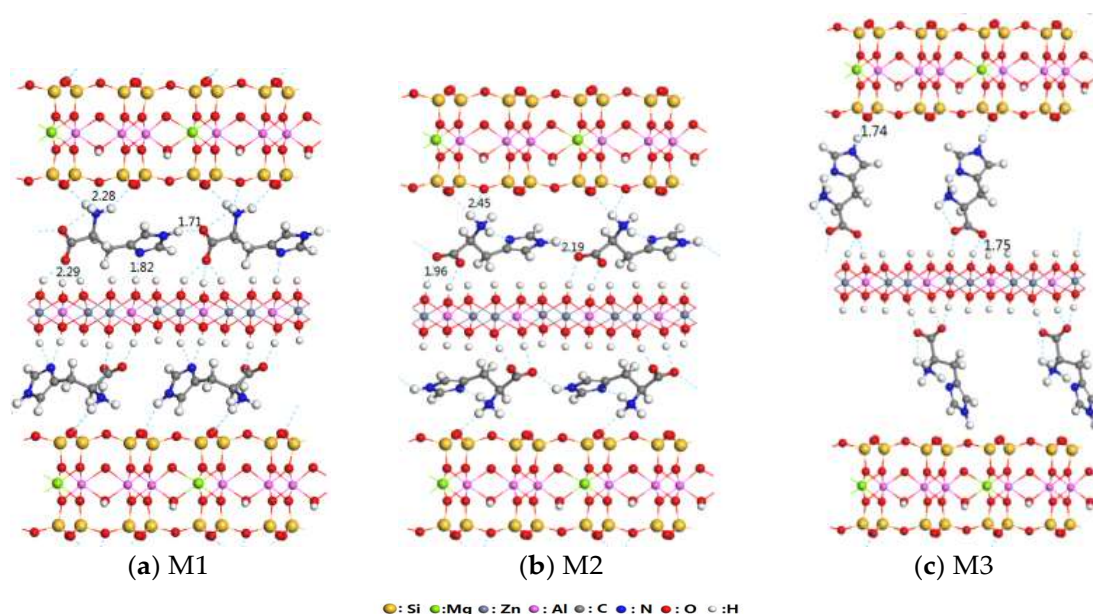


Figure 1. Three structures of His–LDHs–MMT (M1, M2, M3) (cell composition: $a \times 2b \times c$).

Table 1. Lattice parameters and energy of M1, M2, and M3.

	a (nm)	c (nm)	Energy/Ha
M1	0.53	2.27	−14,666.2078
M2	0.53	2.26	−14,666.1890
M3	0.53	2.98	−14,666.0605

3.2. Interaction of Interlayer Guest of His-LDHs-MMT Complex

As is clear from Figure 1, some interactions may exist between the interlayer guests of M1 and M2. In order to determine the interaction, M4 is constructed on the basis of M1 after removing the LDH, MMT lamellae and fixing the unit cell parameters, as shown in Figure 2. By analyzing and computing the complex structure and the unit cell data, the interaction between the His guests is shown to exist in the same layer, so the guest interaction between different layers is neglected. The computed energy of M4 is -1097.6171 Ha, and two kinds of His guests in the unit cell are -548.7712 and -548.7501 Ha, respectively. The interaction energy of interlayer guests is -60.08 kcal/mol, calculated by Equation (1). The computing result shows that the interactions between interlayer guests are very strong. Two histidines in the unit cell both cause the interaction of interlayer guest, and the average interaction energy for histidine is -30.04 kcal/mol computing by Equation (2). This interaction energy is higher than that of the general hydrogen bonding, so it is thought that strong electrostatic interactions maybe exist in the intercalated materials.

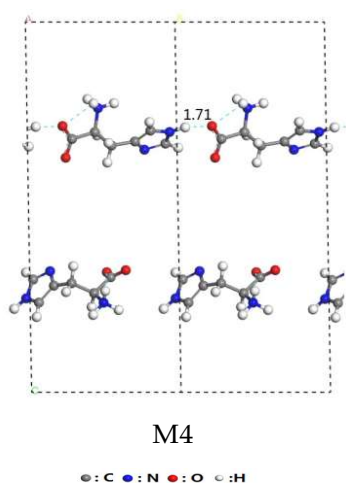


Figure 2. Structural model of histidine guest molecules ($a \times 2b \times c$).

3.3. Interaction of His-LDHs and His-MMT

In order to study the host-guest interaction of His-LDHs-MMT complex, one first needs to know the interaction between His-LDHs and His-MMT. The structural models of histidine-intercalated LDHs and MMT are established on the basis of charged characteristics of intercalated materials, respectively. By studying the interaction of histidine with LDHs and MMT, the combination strength of the histidine and two lamellae is analyzed, and the stability of histidine in the LDHs-MMT complex is further determined.

M5 shown in Figure 3a gives the structure of histidine-intercalated LDHs. There are two LDHs lamellae and four histidine zwitterions. It can be seen that the LDHs layers are linked by the oxygen atom of histidine carboxylate to the hydrogen of LDHs. The space group symmetry of M5 belongs to P1. The unit cell parameters a and c are 0.62 and 2.76 nm, respectively. The interatomic distance of H–O is about 1.64–1.87 Å, which belongs to the range of hydrogen bond length. When histidine is intercalated into the LDHs, the carboxylate of each histidine is adsorbed on the Al–O–H site of the Zn–Al LDHs lamella. M5-1 shown in Figure 3b is the fixed structure of pure LDHs lamellae after removing histidine molecule and retaining the unit cell parameters of M5. There are two lamellae in the unit cell. M5-2 shown in Figure 3c is the fixed structure of histidine after removing LDHs lamellae and retaining the M5-1 unit cell parameters of M5. There are four histidine zwitterions in the M5-2 unit cell. The energies of M5, M5-1, and M5-2 are about $-26,949.2076$, $-24,753.4371$, and -2195.3537 Ha, respectively. Therefore, the binding energy of histidine-intercalated LDHs lamellae is -261.54 kcal/mol, calculated using Equation (3). The average binding energy per amino acid is

−65.38 kcal/mol, calculated using Equation (4). The interaction of histidine-intercalated LDHs lamellae is so strong that the intercalation structure is very stable.

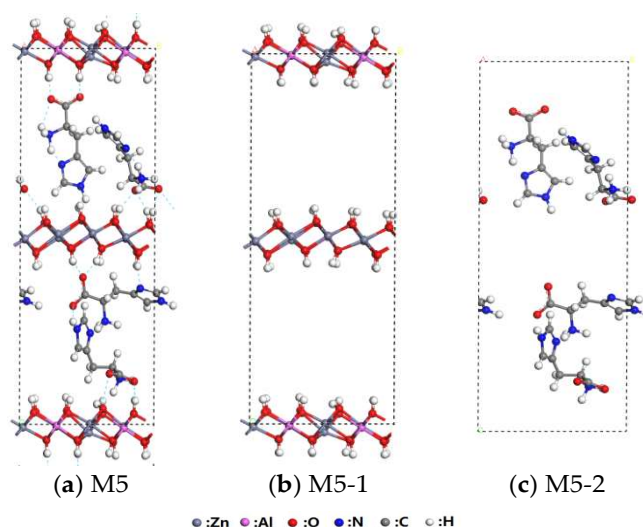


Figure 3. Structural models of histidine intercalated LDHs; (a): histidine-intercalated LDHs structure; (b): LDHs lamellas structure; (c): histidines structure in M5.

M6 shown in Figure 4a gives the structure of histidine-intercalated MMT. There is one MMT lamella and two histidine zwitterions. It is obvious that the hydrogen of histidine quaternary ammonium group is linked to the oxygen of MMT. The space group symmetry of M6 also belongs to P1. Its unit cell parameters are $a = 0.54$ nm, $c = 1.8$ nm. The interatomic distance of H–O is about 2.1 Å, which belongs to the category of hydrogen bond. Under the premise of retaining M6 original cell data, M6-1 shown in Figure 4b is the fixed structure of MMT lamellae after removing histidine zwitterions. M6-2 shown in Figure 4c is the fixed histidine zwitterions after removing the MMT lamella and retaining the unit cell parameters of M5 structure. The total energies of M6, M6-1 and M6-2 are −11,202.9512, −10,105.4292, and −1097.2752 Ha, respectively. The binding energy of histidine and MMT lamellas is −154.87 kcal/mol, according to Equation (3). The average energy of per histidine intercalated montmorillonite is −77.43 kcal/mol, according to Equation (4). The interaction energy of His intercalated MMT is so high that the intercalated structure should be stable.

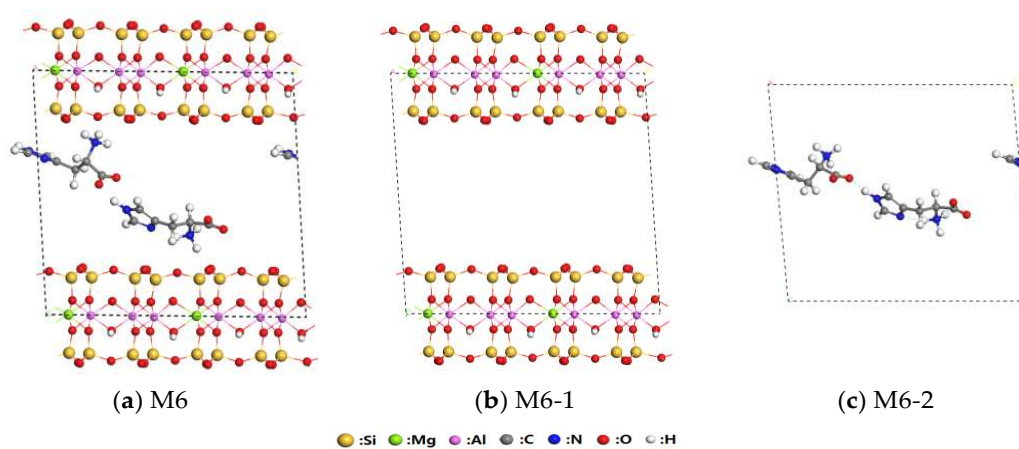


Figure 4. Structural models of histidine intercalated MMT; (a): histidine-intercalated MMT structure; (b): MMT lamellas structure; (c): histidines structure in M6.

3.4. Interaction of His-LDHs-MMT Complex

The energy of M1 is the lowest in the three kinds of complex structures. The host structure of M1 and M2 is almost same. The interlayer spacing of M3 is the largest, and its energy is the highest. According to these analyses of the His-LDHs-MMT complex structure, the interaction of M1 structure is selected to study the interaction of histidine with LDH, MMT, and complex. In order to determine the interaction of His with LDHs and MMT lamellae, the structural models of LDHs-MMT(M1-1) and His(M1-2) shown in Figure 5 are established on the base of M1 removing guest or host and retained other atomic position, respectively. The energy of M1-1 and M1-2 is $-13,568.0269$ and -1097.6171 Ha, respectively. The intercalation energy of His with LDHs-MMT complex is -353.84 kcal/mol calculated by Equation (3), and the average energy of each histidine intercalated LDHs-MMT is -176.92 kcal/mol. It can be seen from the above calculation data that the interaction of His-LDHs-MMT is strong, and stable intercalation complexes can be formed theoretically.

The calculated binding energies of histidine with LDHs and MMT are much higher than the energy of the general hydrogen bonds. The combination of histidine and MMT is mainly dominated by electrostatic adsorption, whereas histidine and LDHs are mainly bounded by hydrogen bonding. On the other hand, since the complex is a combination of charged groups, the rest of energy may come from the electrostatic interaction. Analyzing the composition of interaction energy, it is thought that the electrostatic interaction in LDHs and MMT should be a large component besides the hydrogen bonding interaction between the guest and the host lamella. The host-guest interaction energy of His-LDHs-MMT is about the sum of the interaction energies of His-LDHs and His-MMT. It is shown that histidine has a strong interaction with both hydrotalcite and montmorillonite lamellae. Therefore, histidine can be stably intercalated into the lamellae of LDHs-MMT.

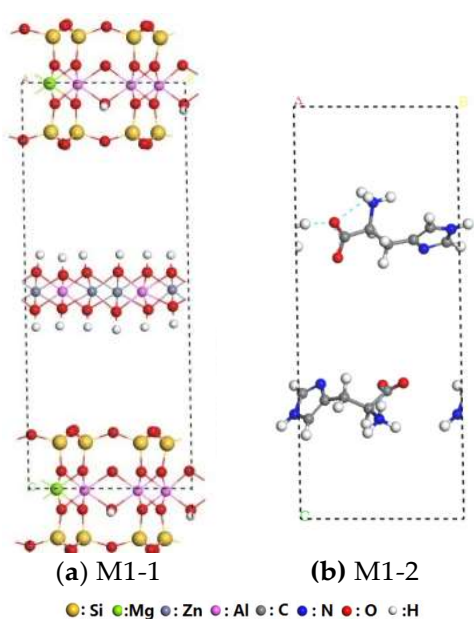


Figure 5. Structural models of LDHs-MMT lamellae and histidine; (a): LDHs-MMT structure; (b): histidine structure in M1.

3.5. Electronic Structural Property of His-LDHs-MMT

The electronic properties of the complex, such as XRD, density of states, charge density, and electrostatic potentials, can help us to understand the stability and internal structure of the complex.

The XRD patterns of complex model are simulated shown in Figure 6. The M1 strongest diffraction peak (001) of MMT lamella appears at $2\theta = 7.8^\circ$; the (003) peak and (110) bimodal peak of LDHs lamella occur at $2\theta = 11.7^\circ, 60^\circ$, respectively. Other peak types are basically a combination of peak shapes

of MMT and LDHs. It is similar to the XRD spectra of p-aminobenzene sulfonic acid intercalated LDHs–MMT complex in the literature [44]. The obtained characteristic peaks of the intercalation complexes from the above XRD spectrum simulation may provide some theoretical references for the experimental testing of material structure.

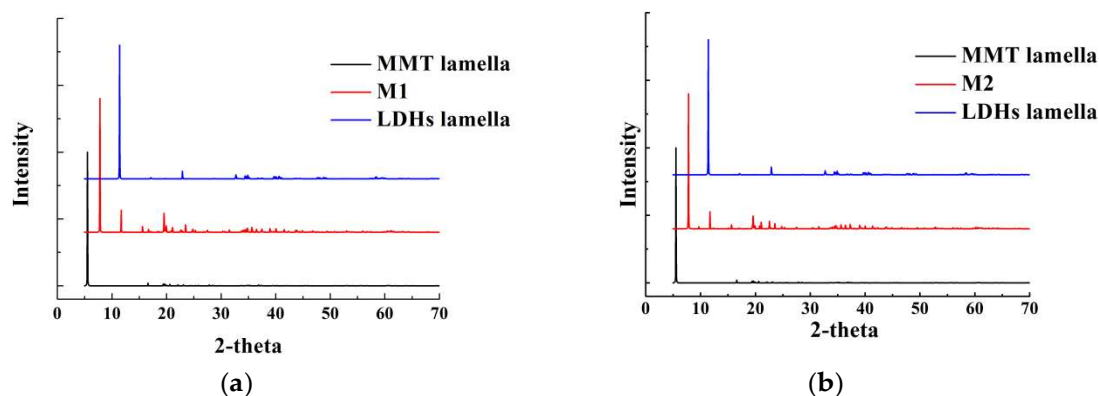


Figure 6. XRD Simulation of different material structures (using Cu K-alpha radiation); (a): XRD pattern of M1, MMT and LDHs; (b): XRD pattern of M2, MMT and LDHs.

In order to explain the interactions of the guests with hosts in the complexes, the partial density of states (PDOS) of the O–H and N–H bonds bound to the zwitterions and layers are calculated for M1 and M2, as shown in Figure 7. A clear orbital overlap can be found in the PDOS, indicating the existence of certain interaction at this energy level. For M1 and M2, the results show that the lowest orbital distribution at about -21.56 eV is mostly formed with the H 1s electrons, with a minor degree of O 2p states. Near the Fermi level, the orbital contribution consists of p electrons of O atom and s electrons of H atom, indicating a strong interaction (i.e., that a hydrogen bond function existed in the complex).

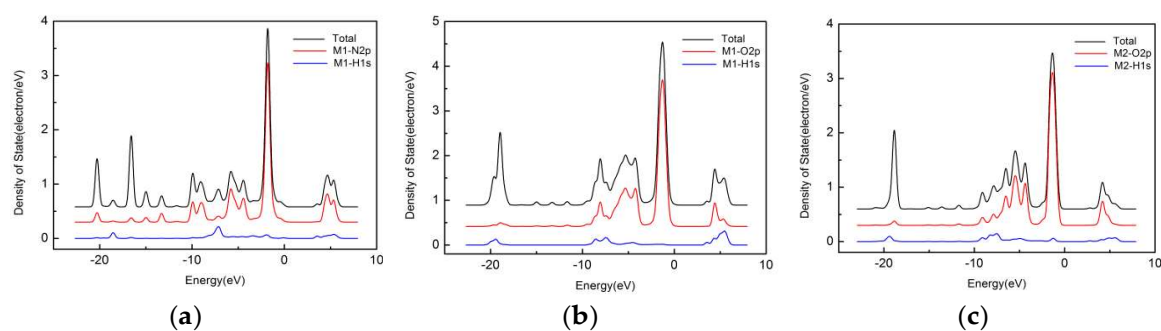


Figure 7. The PDOS curves of M1, M2 structures; (a): O–H PDOS curves of M1; (b): N–H PDOS curves of M1; and c: O–H PDOS curves of M2.

In the charge density diagram, histidine is combined with LDH and MMT lamellae using hydrogen bonds with the different strengths, as shown in Figure 8. The density field of LDHs overlaps with histidine, indicating that a strong interaction exists between histidine and LDHs. However, there is not electron distribution overlap between histidine and the MMT lamella, which indicates that the bonding effects are weaker than those of LDHs, and most of the interaction is electrostatic force. Meanwhile, a strong interaction of the indole ring nitrogen atoms and the LDHs is formed in the M1 geometry.

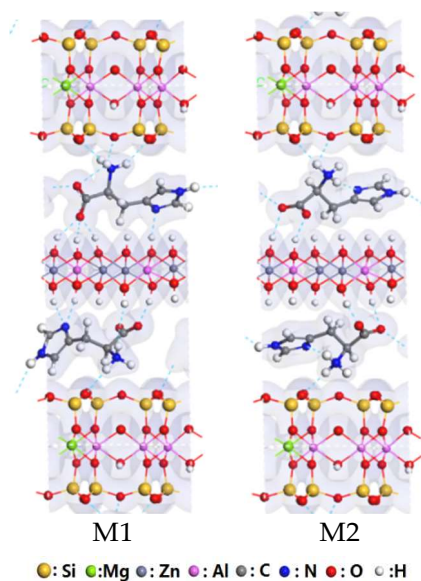


Figure 8. Simulations of charge density of M1 and M2.

The electrostatic potential of molecule is suitable for analyzing the weak interactions dominated by static electricity. As shown in Figure 9, the electrostatic potential of MMT lamella is higher than that of LDHs. It is indicated that the electrostatic effect of MMT lamella is strong. In addition, the carboxyl group of histidine also represents a certain electrostatic potential, so that there is some electrostatic interaction between histidine and LDHs. It is shown that the electrostatic interaction between histidine and MMT lamella is much stronger than that of LDHs. The above analysis confirms the main combination modes of histidine with different lamellae are electrostatic adsorption of His with MMT and hydrogen bonding of His with LDHs.

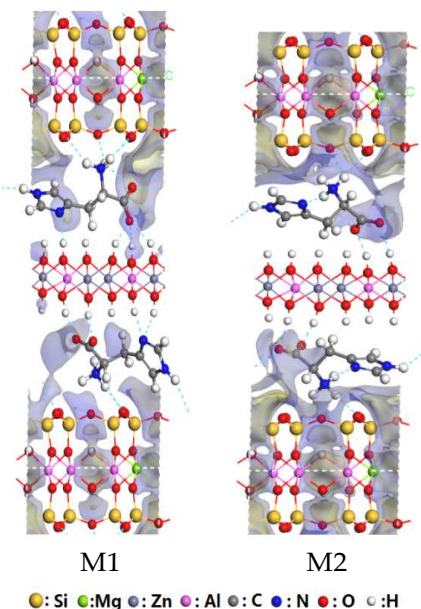


Figure 9. Simulations of electrostatic potentials of M1 and M2.

4. Conclusions

A special type of intercalated structure with the histidine(His) zwitterions and alternating hydrotalcite–montmorillonite lamellae was explored using the density functional theory (DFT) of quantum chemistry. By analyzing complex structure, it is determined that the amphoteric charged characteristics of host and guest adapt to the preparation of intercalated materials using the self-assembly method. The simulations of complex (His–LDHs–MMT) structures show that amino group of histidine is adsorbed with the oxygen of the MMT lamella, and the oxygen on the carboxyl groups is combined with the hydrogen atoms of the LDHs lamella. The binding energy of His–LDHs–MMT is -353.84 kcal/mol, and its average histidine binding energy is -176.92 kcal/mol. The binding energy of per histidine intercalated LDHs and MMT is -65.89 and -78.44 kcal/mol, respectively. These values include the electrostatic and hydrogen bond interactions. The calculated results show that histidine may be stably intercalated between the LDHs and MMT by a supramolecular interaction. The properties analysis of the complex structure can accurately reflect the distribution of electrons. The PDOS shows that orbital contributions of H 1s and O 2p overlap near the Fermi level, confirming the presence of hydrogen bonds in the complex. In the charge density, the bonding effect of histidine with LDHs lamella is stronger than that with MMT lamella, as there is an overlap of the density field of histidine with LDHs lamella but no overlap of that of MMT. According to the electrostatic potential analysis of the complex, the electrostatic force of histidine with MMT lamella is stronger than that of LDHs. The above analysis shows that the binding of histidine with MMT is mainly dominated by electrostatic force, whereas that of histidine and LDHs is mainly produced by the hydrogen bond. The computation results of the electronic properties and host-guest interactions confirm that the intercalated complexes should be prepared experimentally.

Author Contributions: Chen-Xi Wang has finished the main work and wrote the initial draft of this paper. Min Pu is the supervisor that has advised Chen-Xi Wang, Pei-Huan Zhang and Yang Gao during the course of this work. Pei-Huan Zhang and Yang Gao participated the revision of article and analysis of data. Zuo-Yin Yang and Ming Lei gave the meaningful guidance and analysis of computational results.

Acknowledgments: This project was supported by the National Natural Science Foundation of China (21173019).

Conflicts of Interest: The authors declare no conflict of interest.

References

1. Ai, L.; Zhang, C.; Meng, L. Adsorption of methyl orange from aqueous solution on hydrothermal synthesized Mg–Al layered double hydroxide. *J. Chem. Eng. Data* **2011**, *56*, 4217–4225. [[CrossRef](#)]
2. Lee, G.; Jeong, Y.; Takagaki, A.; Jung, J.C. Sonication assisted rehydration of hydrotalcite catalyst for isomerization of glucose to fructose. *J. Mol. Catal. A Chem.* **2014**, *393*, 289–295. [[CrossRef](#)]
3. Serio, M.D.; Mallardo, S.; Carotenuto, G.; Tesser, R.; Santacesaria, E. Mg/Al hydrotalcite catalyst for biodiesel production in continuous packed bed reactors. *Catal. Today* **2012**, *195*, 54–58. [[CrossRef](#)]
4. Wang, Y.B.; Jehng, J.M. Hydrotalcite-like compounds containing transition metals as solid base catalysts for transesterification. *Chem. Eng. J.* **2011**, *175*, 548–554. [[CrossRef](#)]
5. Dadwhal, M.; Sahimi, M.; Tsotsis, T.T. Adsorption isotherms of arsenic on conditioned layered double hydroxides in the presence of various competing ions. *Ind. Eng. Chem. Res.* **2011**, *50*, 2220–2226. [[CrossRef](#)]
6. Rives, V.; Arco, M.; Martin, C. Layered double hydroxides as drug carriers and for controlled release of non-steroidal antiinflammatory drugs (NSAIDs): A review. *J. Control. Release* **2013**, *169*, 28–39. [[CrossRef](#)] [[PubMed](#)]
7. Vial, S.; Prevot, V.; Lerous, F.; Forano, C. Immobilization of urease in ZnAl layered double hydroxides by soft chemistry routes. *Microporous Mesoporous Mater.* **2008**, *107*, 190–201. [[CrossRef](#)]
8. Tarutani, N.; Tokudome, Y.; Jobbagy, M.; Viva, F.A.; Soler-Illia, G.J.A.A.; Takahashi, M. Single-nanometer-sized low-valence metal hydroxide crystals: Synthesis via epoxide-mediated alkanization and assembly toward functional mesoporous materials. *Chem. Mater.* **2016**, *28*, 5606–5610. [[CrossRef](#)]
9. Dewoolkar, K.D.; Vaidya, P.D. Tailored Ce- and Zr-doped Ni/hydrotalcite materials for superior sorption-enhanced steam methane reforming. *Int. J. Hydrogen Energy* **2017**, *42*, 21762–21774. [[CrossRef](#)]

10. Stawinski, W.; Wegrzyn, A.; Freitas, O.; Chmielarz, L.; Figueiredo, S. Dual-function hydrotalcite-derived adsorbents with sulfur storage properties: Dyes and hydrotalcite fate in adsorption-regeneration cycles. *Microporous Mesoporous Mater.* **2017**, *250*, 72–87. [[CrossRef](#)]
11. Anirudhan, T.S.; Suchithra, P.S. Synthesis and characterization of tannin-immobilized hydrotalcite as a potential adsorbent of heavy metal ions in effluent treatments. *Appl. Clay Sci.* **2008**, *42*, 214–223. [[CrossRef](#)]
12. Park, Y.; Ayoko, G.A.; Frost, R.L. Application of organoclays for the adsorption of recalcitrant organic molecules from aqueous media. *J. Colloid Interface Sci.* **2011**, *354*, 292–305. [[CrossRef](#)] [[PubMed](#)]
13. Wang, C.; Li, Z. Cation exchange interaction between antibiotic ciprofloxacin and montmorillonite. *J. Hazard. Mater.* **2010**, *183*, 309–314. [[CrossRef](#)] [[PubMed](#)]
14. Gemeay, A.H.; El-Sherbiny, A.S.; Zaki, A.B. Adsorption and kinetic studies of the intercalation of some organic compounds onto Na⁺-montmorillonite. *J. Colloid Interface Sci.* **2002**, *245*, 116–125. [[CrossRef](#)] [[PubMed](#)]
15. Sahoo, P.K.; Samal, R.F. Fire retardancy and biodegradability of poly(methyl methacrylate)/montmorillonite nanocomposite. *Polym. Degrad. Stab.* **2007**, *92*, 1700–1702. [[CrossRef](#)]
16. Kan, T.; Jiang, X.; Zhou, L.; Yang, M.; Duan, M. Removal of methyl orange from aqueous solutions using a bentonite modified with a new gemini surfactant. *Appl. Clay Sci.* **2011**, *54*, 184–187. [[CrossRef](#)]
17. Liu, K.; Liu, T.; Chen, S.; Liu, D. Drug release behavior of chitosan–montmorillonite nanocomposite hydrogels following electrostimulation. *Acta Biomater.* **2008**, *4*, 1038–1045. [[CrossRef](#)] [[PubMed](#)]
18. Zaghouane-Boudiaf, H.; Boutahala, M. Adsorption of 2,4,5-trichlorophenol by organo-montmorillonites from aqueous solutions: Kinetics and equilibrium studies. *Chem. Eng. J.* **2011**, *170*, 120–126. [[CrossRef](#)]
19. Park, J.H.; Shin, H.J.; Kim, M.H.; Kim, J.S.; Kang, N.; Lee, J.Y.; Kim, K.T.; Lee, J.I.; Kim, D.D. Application of montmorillonite in bentonite as a pharmaceutical excipient in drug delivery systems. *J. Pharm. Investig.* **2016**, *46*, 363–375. [[CrossRef](#)]
20. Terry, P.A. Characterization of Cr ion exchange with hydrotalcite. *Chemosphere* **2004**, *57*, 541–546. [[CrossRef](#)] [[PubMed](#)]
21. Goh, K.; Lim, T.; Dong, Z. Application of layered double hydroxides for removal of oxyanions: A review. *Water Res.* **2008**, *42*, 1343–1368. [[CrossRef](#)] [[PubMed](#)]
22. Barriga, C.; Gaitan, M.; Pavlovic, I. Hydrotalcites as sorbent for 2,4,6-trinitrophenol: Influence of the layer composition and interlayer anion. *J. Mater. Chem.* **2002**, *12*, 1027–1032. [[CrossRef](#)]
23. Pu, M.; Su, Y.; Zhang, X.F.; He, S.H. An Amino Acid Compound Assembled Montmorillonite-Hydrotalcite Layered Material and Preparation Method. China ZL 2013 101421982, 22 April 2013.
24. Scheffler, U.; Mahrwald, R. Histidine-catalyzed asymmetric aldol addition of enolizable aldehydes: Insights into its mechanism. *J. Org. Chem.* **2012**, *77*, 2310–2330. [[CrossRef](#)] [[PubMed](#)]
25. Lam, Y.H.; Houk, K.N.; Scheffler, U.; Mahrwald, R. Stereoselectivities of histidine-catalyzed asymmetric aldol additions and contrasts with proline catalysis: A quantum mechanical analysis. *J. Am. Chem. Soc.* **2012**, *134*, 6286–6295. [[CrossRef](#)] [[PubMed](#)]
26. Guo, P.F.; Wei, Q.Y.; Jiang, H.; Xie, P.F. L-proline and L-histidine co-catalyzed Baylis–Hillman reaction. *Res. Chem. Intermed.* **2012**, *38*, 639–644. [[CrossRef](#)]
27. Liu, X.X.; Melman, A. Templated alkylation of hexahistidine with Baylis–Hillman esters. *Chem. Commun.* **2013**, *49*, 9042–9044. [[CrossRef](#)] [[PubMed](#)]
28. Mulder, D.T.; McPhee, J.B.; Yu, S.A.R.; Stogios, P.J.; Savchenko, A.; Coombes, B.K. Multiple histidines in the periplasmic domain of the Salmonella enterica sensor kinase SsrA enhance signaling in response to extracellular acidification. *Mol. Microbiol.* **2015**, *95*, 678–691. [[CrossRef](#)] [[PubMed](#)]
29. Rashid, Z.; Naeimi, H.; Zarnani, A.H.; Mohammadi, F.; Ghahremanzadeh, R. Facile fabrication of nickel immobilized on magnetic nanoparticles as an efficient affinity adsorbent for purification of his-tagged protein. *Mater. Sci. Eng. C* **2017**, *80*, 670–676. [[CrossRef](#)] [[PubMed](#)]
30. Lin, Y.W.; Dong, S.S.; Liu, J.H.; Nie, C.M.; Wen, G.B. Peroxidase activity of a myoglobin mutant with three distal histidines forming a metal-binding site: Implications for the cross-reactivity of cytochrome c oxidase. *J. Mol. Catal. B Enzym.* **2013**, *91*, 25–31. [[CrossRef](#)]
31. Dong, S.S.; Du, K.J.; You, Y.; Liu, F.; Wen, G.B.; Lin, Y.W. Peroxidase-like activity of L29H myoglobin with two cooperative distal histidines on electrode using O₂ as an oxidant. *J. Electroanal. Chem.* **2013**, *708*, 1–6. [[CrossRef](#)]

32. Mahindra, A.; Jain, R. Regiocontrolled palladium-catalyzed and copper-mediated C–H bond functionalization of protected L-histidine. *Org. Biomol. Chem.* **2014**, *12*, 3792–3796. [[CrossRef](#)] [[PubMed](#)]
33. Mahindra, A.; Bagra, N.; Jain, R. Palladium-catalyzed regioselective C-5 arylation of protected L-histidine: Microwave-assisted C-H activation adjacent to donor arm *Org. Chem.* **2013**, *78*, 10954–10959. [[CrossRef](#)] [[PubMed](#)]
34. Liu, M.; Zhang, Z.; Cheetham, J.; Ren, D.; Zhou, Z.S. Discovery and characterization of a photo-oxidative histidine-histidine cross-link in IgG1 antibody utilizing 18O-Labeling and mass spectrometry. *Anal. Chem.* **2014**, *86*, 4940–4948. [[CrossRef](#)] [[PubMed](#)]
35. Vu, A.P.; Mnguyen, T.N.; Do, T.T.; Doan, T.H. Clinical screening of paraquat in plasma samples using capillary electrophoresis with contactless conductivity detection: Towards rapid diagnosis and therapeutic treatment of acute paraquat poisoning in Vietnam. *J. Chromatogr. B* **2017**, *1060*, 111–117. [[CrossRef](#)] [[PubMed](#)]
36. Moti, M.; Ishikawara, F.; Tomoda, T.; Yamada, S. Use of capillary electrophoresis with dual-opposite end injection for simultaneous analysis of small ions in saliva samples from wrestlers undergoing a weight training program. *J. Chromatogr. B* **2016**, *1012–1013*, 178–185.
37. Aisawa, S.; Sasaki, S.; Takahashi, S.; Hirahara, H.; Nakayama, H.; Narita, E. Intercalation of amino acids and oligopeptides into Zn–Al layered double hydroxide by coprecipitation reaction. *J. Phys. Chem. Solids* **2006**, *67*, 920–925. [[CrossRef](#)]
38. Nakayama, H.; Wada, N.; Tshako, M. Intercalation of amino acids and peptides into Mg–Al layered double hydroxide by reconstruction method. *Int. J. Pharm.* **2004**, *269*, 469–478. [[CrossRef](#)] [[PubMed](#)]
39. Whilton, N.T.; Vickers, P.J.; Mann, S. Bioinorganic clays: Synthesis and characterization of amino- and polyamino acid intercalated layered double hydroxides. *J. Mater. Chem.* **1997**, *7*, 1623–1629. [[CrossRef](#)]
40. Fudala, A.; Pálíno, I.; Kiricsi, I. Preparation and characterization of hybrid organic-inorganic composite materials using the amphoteric property of amino acids: Amino acid intercalated layered double hydroxide and montmorillonite. *Inorg. Chem.* **1999**, *38*, 4653–4658. [[CrossRef](#)]
41. Yuan, Q.; Wei, M.; Evans, D.G.; Duan, X. Preparation and investigation of thermolysis of L-aspartic acid-intercalated layered double hydroxide. *J. Phys. Chem. B* **2004**, *108*, 12381–12387. [[CrossRef](#)]
42. Kitadai, N.; Yokoyama, T.; Nakashima, S. In situ ATR-IR investigation of L-lysine adsorption on montmorillonite. *J. Colloid Interface Sci.* **2009**, *338*, 395–401. [[CrossRef](#)] [[PubMed](#)]
43. Mallakpour, S.; Dinari, M. Insertion of novel optically active poly(amide-imide) chains containing pyromellitoyl-bis-L-phenylalanine linkages into the nanolayered silicates modified with L-tyrosine through solution intercalation. *Polymer* **2011**, *51*, 2514–2523. [[CrossRef](#)]
44. Fraser, D.G.; Greenwell, C.; Skipper, N.; Smalley, M.V.; Wilkinson, M.A.; Deme, B.; Heenan, R.K. Chiral interactions of histidine in a hydrated vermiculite. *Phys. Chem. Chem. Phys.* **2011**, *13*, 825–830. [[CrossRef](#)] [[PubMed](#)]
45. Songurtejn, D.; Yalcinlaya, E.E.; Ag, D.; Seleci, M.; Demirkol, D.O. Histidine modified montmorillonite: Laccase immobilization and application to flow injection analysis of phenols. *Appl. Clay Sci.* **2013**, *68*, 64–69. [[CrossRef](#)]
46. He, S.H.; Pu, M.; Zhang, X.F.; Wang, C.X.; Wang, H.X. Analysis and simulations on the structure of sulfanilic acid zwitterion intercalated hydrotalcite and montmorillonite. *RSC Adv.* **2016**, *6*, 83656–83662. [[CrossRef](#)]
47. Delley, B. From molecules to solids with the DMol3 approach. *J. Chem. Phys.* **2000**, *113*, 7756–7763. [[CrossRef](#)]
48. Delley, B. An all-electron numerical method for solving the local density functional for polyatomic molecules. *J. Chem. Phys.* **1990**, *92*, 508–517. [[CrossRef](#)]

